Lab on a Chip

Cite this: *Lab Chip*, 2012, **12**, 1078

www.rsc.org/loc

PAPER

Design considerations for electrostatic microvalves with applications in poly(dimethylsiloxane)-based microfluidics†

Amit V. Desai,[a] Joshua D. Tice,[a] Christopher A. Apblett[bc] and Paul J. A. Kenis*[a]

Received 19th November 2011, Accepted 17th January 2012
DOI: 10.1039/c2lc21133e

Microvalves are critical in the operation of integrated microfluidic chips for a wide range of applications. In this paper, we present an analytical model to guide the design of electrostatic microvalves that can be integrated into microfluidic chips using standard fabrication processes and can reliably operate at low actuation potentials (<250 V). Based on the analytical model, we identify design guidelines and operational considerations for elastomeric electrostatic microvalves and formulate strategies to minimize their actuation potentials, while maintaining the feasibility of fabrication and integration. We specifically explore the application of the model to design microfluidic microvalves fabricated in poly(dimethylsiloxane), using only soft-lithographic techniques. We discuss the electrostatic actuation in terms of several microscale phenomena, including squeeze-film damping and adhesion-driven microvalve collapse. The actuation potentials predicted by the model are in good agreement with experimental data obtained with a microfabricated array of electrostatic microvalves actuated in air and oil. The model can also be extended to the design of peristaltic pumps for microfluidics and to the prediction of actuation potentials of microvalves in viscous liquid environments. Additionally, due to the compact ancillaries required to generate low potentials, these electrostatic microvalves can potentially be used in portable microfluidic chips.

Introduction

The advent of very large scale integration (VLSI) microfluidics has enabled multi-step and high-throughput applications with massively parallel operations to be performed on a single chip.[1,2] Key to these advances was the development of pneumatic microvalves,[3] which are fabricated with soft-lithographic techniques and are based on the actuation of a thin polymeric membrane by pressurized air. Despite successful integration of such pneumatic microvalves in microfluidic chips for diverse applications, these microvalves require bulky ancillaries including a pressure source and external solenoid valves, which limit the scalability and portability of these microfluidic chips. Numerous other microvalve technologies have been reported over the years, many of which are summarized in a recent review.[4] These valves can be broadly classified as active microvalves (*e.g.*, electrostatic or pneumatic microvalves) and passive microvalves (*e.g.*, capillary force-based[4] and surface hydrophobicity-based valves[5]). However, few of these valve technologies are amenable to integration into complex microfluidic chips due to the intensive nature of the required fabrication procedures, actuation crosstalk between adjacent valves, and/or incompatibility of the valve actuation principle with all the chemical and biological processes on-chip.

Microvalves based on electrostatic actuation retain the small footprint (<500 μm) and fast response time (<1 s) of their pneumatic equivalents, while requiring less bulky ancillaries, which greatly improves portability and scalability. Although electrostatic actuation has been frequently used to operate valves in microelectromechanical systems (MEMS) made out of hard materials (*e.g.* silicon, glass), very few reports of electrostatic microfluidic valves, typically made out of soft polymeric materials, exist in literature. Chang and Maharbiz[6] used electrostatic actuation to operate pumps and valves in poly(dimethylsiloxane) (PDMS) microfluidic chips, while Xie *et al.*[7] developed a surface-micromachined peristaltic pump in parylene based on electrostatic actuation. These valves or pumps are typically fabricated using a combination of integrated circuit (IC) fabrication procedures (photolithography, metal and oxide deposition, and etching) and soft-lithographic processes (polymer molding). While many of these valves can be integrated on a single chip, the fact that complex and intensive IC fabrication processes are required for their manufacture has limited their use.

[a]*Department of Chemical & Biomolecular Engineering, University of Illinois at Urbana-Champaign, 600 South Mathews Avenue, Urbana, IL 61801, USA. E-mail: kenis@illinois.edu; Fax: +01 217 333-5052; Tel: +01 217 265-0523*
[b]*Sandia National Laboratories, P.O. Box 5800, Albuquerque, NM 87185, USA*
[c]*Department of Chemical & Nuclear Engineering, University of New Mexico, Albuquerque, NM 87131, USA. E-mail: caapble@sandia.gov*
† Electronic supplementary information (ESI) available. See DOI: 10.1039/c2lc21133e

Two key challenges need to be addressed to develop microfluidic valves based on electrostatic actuation. First, the fabrication and integration of these valves should be compatible with standard soft-lithographic processes. As a result, the microvalve dimensions (*e.g.*, thickness of insulating layers) will be almost an order larger than those in typical MEMS devices due to fabrication limitations imposed by soft lithography. The relatively larger microvalve dimensions achievable by soft-lithographic processes places a lower limit on the achievable actuation potentials. Second, due to the high surface energies of polymers, the microfluidic valves tend to collapse during fabrication and/or operation. This adhesion-driven collapse not only restricts the allowable microvalve dimensions for reliable and robust operation, but also enforces a lower limit on the actuation potentials.

To address the above challenges, we use analytical modeling to guide the design of electrostatic microfluidic microvalves with respect to feasibility of fabrication and integration (using only soft-lithographic processes) and reliable and robust operation (minimizing microvalve adhesion during operation) at low actuation potentials. The operation of the proposed electrostatic microvalve is based on the deformation of a flexible membrane due to electrostatic forces, which involves several physical phenomena, such as coupling between mechanical deformation and electric fields, static and dynamic deformation in viscous and pressurized fluids, and adhesion-driven collapse of membranes. A systematic model that captures the interplay of these phenomena is needed to accurately describe the microvalve operation and to guide subsequent optimization of the microvalve design, with the objective of minimizing actuation potentials while maintaining fabrication simplicity and feasibility. The model-based design becomes especially important for microvalves that can be actuated with low potentials (*e.g.* in portable microfluidic applications), since any effort to decrease the actuation potential compromises the reliability and robustness of the microvalve (*e.g.*, collapse of the valves during operation).

We extend analytical models reported in the literature to microfluidic applications by considering several issues that are typically ignored in electrostatic actuation of microscale structures, such as the use of multi-layer components, collapse of valve membranes, and dynamic actuation in pressurized liquids. Although the analytical model is described within a generic framework, we specifically focus on the design of microfluidic valves fabricated out of soft polymers (*e.g.*, PDMS), which are key towards the development of VLSI microfluidics, in contrast to most of the literature that discusses electrostatic microvalves fabricated out of hard materials (*e.g.*, silicon, glass). The analytical model reported here explicitly identifies the critical design parameters from which a set of design guidelines can be derived to address the challenges mentioned above. Microfluidic chips with valves and pumps that can be actuated with low potentials can be used in portable applications, due to the compact ancillaries required for generation of small actuation potentials.

Analytical model

Two approaches are most commonly used in the modeling of electrostatic actuation of microscale structures: (1) numerical techniques, and (2) analytical and semi-analytical approaches. In the former approach, finite element analysis (FEA) or numerical analysis of the governing differential equations has been used to examine the deflection of compliant structures due to electrostatic forces. These studies have analyzed various phenomena during electrostatic actuation, including dynamics of pull-in behavior,[8] effect of large deformation and non-linear material properties,[9] and Casimir forces.[10] However, the non-explicit representation of the design parameters and the complexity of these computational procedures limit the utility of these numerical models for the design of new electrostatic valve configurations. In contrast, analytical and semi-analytical approaches describe the physical relationships between all the geometrical, material and operational parameters explicitly. This approach has been used to model electrostatic actuation in various microscale applications, including actuation of microelectromechanical systems (MEMS) in liquids,[11] and measurements of material properties using electrostatic actuation.[12] In this section, we extend these analytical models to microfluidic applications and develop an analytical model that can be used to qualitatively and quantitatively describe the operation of our proposed electrostatic microvalves.

The electrostatic microvalve configuration proposed in this paper is composed of a thin, flat, and elastomeric membrane suspended above a microfluidic channel and clamped at the outer edges (Fig. 1a). The membrane is coated with a layer of conducting nanoparticles, forming the top electrode, and the channel floor is a stiff conductor, forming the bottom electrode. An applied potential results in an electric field between the electrodes, which in turn causes the electrostatic forces to collapse the membrane onto the channel floor, and thus close the microvalve. We envision that the conducting nanoparticles could

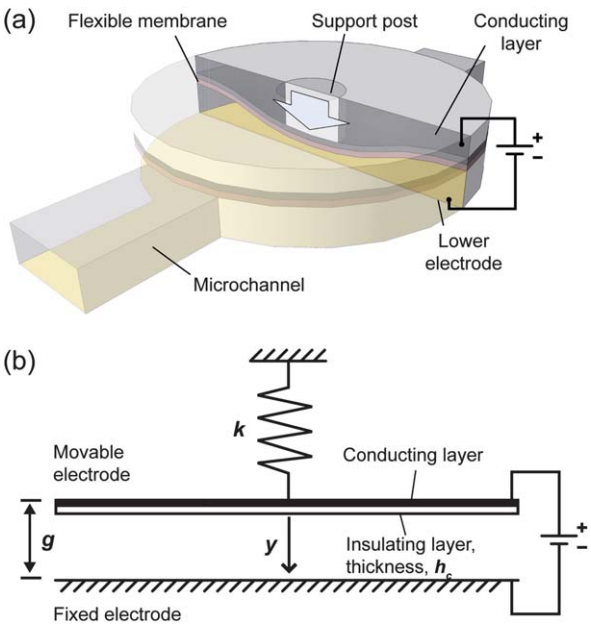

Fig. 1 (a) Schematic illustration of an electrostatic microvalve in a microfluidic channel. (b) Parallel-plate capacitor model for the electrostatic microvalve, with electrode gap/channel height g, spring constant/stiffness of the membrane k, and moveable plate/membrane displacement y.

be patterned *via* micro-transfer printing, and the remainder of the microvalve could be molded from PDMS, allowing the entire fabrication to be accomplished exclusively with soft-lithographic techniques. A thin insulating layer below the upper electrode prevents short-ciruit of the valve in the closed position. The cylindrical support post may be designed into the microvalve configuration to increase the local stiffness of the membrane at the center, which will minimize the probability of adhesion-driven collapse of the valve.

We model the microvalve as a parallel-plate capacitor separated by a distance g, where one plate is movable, resembling the deflecting membrane, and is attached to a spring with spring constant k (Fig. 1b). The parameter y represents the displacement of the membrane and the extension of the spring. In this capacitor system, the electrostatic forces cause the top electrode to move toward the bottom electrode until the electrostatic force is balanced by the tensile force in the spring. First, we derived expressions for the spring constant of the membrane based on plate theory.[13] Next, we calculated the actuation potential for a parallel-plate capacitor system using these spring constant expressions and force-balance equations.

Development of the model: spring constant or stiffness of the membrane

The assumptions made in deriving the expressions for stiffness of the membrane are discussed in the supplementary information, along with the justification. The expression for static stiffness of a square or circular membrane (the two most common geometries for microfluidic microvalves) that is fixed or clamped along the outer edges under a uniformly distributed load is given by

$$k = K_{bilayer}K_{post}\frac{K_{MS}}{K_{AR}}\left(K^1_{shape}\frac{E_{bm}{t_m}^3}{{L_e}^4}+K^2_{shape}\frac{\sigma_0 t_m}{{L_e}^2}\right)$$

$$K_{bilayer} = 1+\frac{E_2{t_2}^3(1-{\nu_m}^2)}{E_m{t_m}^3(1-{\nu_2}^2)} + \frac{3(1-{\nu_m}^2)(1+t_2/t_m)^2(1+E_m t_m/E_2 t_2)}{(1+E_m t_m/E_2 t_2)^2-(\nu_m+\nu_2 E_m t_m/E_2 t_2)^2} \quad (1)$$

where

k static stiffness of the membrane per unit area

E_{bm} biaxial modulus of the membrane and is given by:

$$E_{bm} = \frac{E_m}{1-{\nu_m}^2}$$

E_m Young's modulus of the membrane material

ν_m Poisson's ratio of the membrane material

t_m total thickness of the membrane

σ_0 residual stress in the membrane

L_e equivalent planar dimension of the membrane (side length or diameter)

K^1_{shape} and K^2_{shape} membrane shape factors, *e.g.*, square *vs.* circular[14,15]

K_{AR} factor to account for aspect ratio (AR) and is given by:[13]

$$K_{AR} = 1+\frac{16}{1-\nu_m}\left(\frac{t_m}{L_e}\right)^2$$

K_{MS} factor to account for membrane stresses (MS) and is given by:[13]

$$K_{MS} = 1+0.488\left(\frac{g}{t_m}\right)^2$$

$K_{bilayer}$ factor to account for bilayer configuration[16]

K_{post} factor to account for a cylindrical support post (expression in supplementary information)

E_2 Young's modulus of the material of the second layer

ν_2 Poisson's ratio of the material of the second layer

t_2 thickness of the second layer.

The factor, K_{MS}, accounts for the effect of membrane stresses that develop when the deflection of the membrane exceeds half its thickness. The factor, $K_{bilayer}$, accounts for the fact that membrane properties may not be homogenous along the thickness direction (*e.g.*, due to the presence of an insulating or conducting layer with non-negligible stiffness). In the case of a homogeneous membrane, $K_{bilayer}$ is 1, while for a membrane without a post, K_{post} is 1. Table 1 lists the values of the shape factors for square and circular membranes. Note that, unlike in our analytical treatment here, the effects of aspect ratio, membrane stresses and bilayer membranes (quantified by K_{AR}, K_{MS}, and $K_{bilayer}$, respectively) are typically ignored in the analysis of microfluidic electrostatic microvalves,[6,7,11] which may lead to significant differences between analytical predictions of actuation potentials and experimentally observed values. The expression for stiffness (eqn (1)) represents the stiffness per unit area, because the mechanical loading due to the electrostatic fields is distributed over the entire membrane. If p is the uniform lateral pressure acting on the membrane and y_{max} is the maximum lateral deflection at the center of the membrane, then $p = ky_{max}$.

Development of the model: actuation potential of the microvalve

We used a parallel-plate capacitor model to describe the electrostatic actuation of the microvalve, with one plate fixed and the other attached to a linear spring.[11] In the case of the deflection of a membrane (or any deformable structure) due to forces produced by an electric field, the system becomes unstable when the electrostatic forces and the restoring mechanical forces are no longer in equilibrium.[11] Beyond a certain deflection (critical deflection), the membrane collapses or snaps in (pull-in instability). Depending on the relative magnitudes of the critical deflection and the initial gap between the plates, the operation of the electrostatic valve is either in the stable deflection regime (*i.e.*, critical deflection is never reached) or governed by the aforementioned pull-in instability (*i.e.*, the critical deflection is exceeded). Based on the operation of the valve, the actuation potential to close the valve is given by

Table 1 Shape factors for square and circular membranes

Factor	Square	Circular
K^1_{shape}	66.23[14]	85.33[14]
K^2_{shape}	13.57[15]	16[15]

$$V_{close} = \sqrt{\frac{2kg\left(h_c\frac{\varepsilon_{fluid}}{\varepsilon_m}\right)^2}{\varepsilon_0\varepsilon_{flluid}}} \quad y_{snapin} > g \text{ (stable)}$$
$$V_{close} = \sqrt{\frac{8k\left(g+\left(h_c\frac{\varepsilon_{fluid}}{\varepsilon_m}\right)\right)^3}{27\varepsilon_0\varepsilon_{fluid}}} \quad y_{snapin} \le g \text{ (pull-in)} \qquad (2)$$
$$y_{snapin} = \frac{1}{3}\left(h_c\frac{\varepsilon_{fluid}}{\varepsilon_m}+g\right)$$

where

V_{close} actuation potential required to close the valve

y_{snapin} critical deflection beyond which the electrostatic forces and the restoring mechanical forces are no longer in equilibrium

ε_{fluid} relative permittivity of the fluid

ε_m relative permittivity of the membrane

ε_0 permittivity of free space

h_c thickness of the insulating layer beneath the conducting layer of the top electrode (Fig. 1b)

g initial gap between the plates

k membrane stiffness given by eqn (1).

The assumptions made in deriving the expressions for actuation potential of the microvalve are discussed in the supplementary information, along with the justification.

Development of the model: adhesion-driven collapse of microvalve membranes

An important design consideration for membrane-based microvalves is the collapse of the membrane onto the floor of the channel. Collapse can occur during assembly of the microfluidic chip (self-collapse), or the membranes can remain stuck to the floor even after the actuation potential is removed (operational collapse). This phenomenon of collapse is primarily governed by the interfacial adhesion between the microvalve membrane and the floor of the channel. PDMS-based microfluidic structures sealed to a glass substrate are particularly susceptible to collapse due to their high interfacial adhesion energies with glass (~30–300 mJ m^{-2} in air[17,18]). Note that, although the valves will be actuated primarily in liquids (the surface energies will be lower), the microfluidic devices will be assembled in air, and hence, the adhesion-driven collapse in air will also be an important consideration.

Analytical models for the collapse of free-standing structures due to interfacial adhesion are available for the case of micromachined silicon-based structures and MEMS.[19–21] The collapse of free-standing structures is commonly referred to as the 'stiction' phenomenon. In these models, a dimensionless parameter Ψ (also referred to as elastocapillary number) is derived to predict whether a specific valve collapses or not during actuation.[20–22] When Ψ is less than 1, the valves will collapse due to the interfacial adhesion, whereas valves characterized by a higher value of Ψ do not collapse. Here, we modified the equation for Ψ[21] by integrating the effects of multilayer (K_{bilayer}) and high aspect ratio (K_{AR}) membranes with a cylindrical support post (K_{post}), so that the equation applies to the collapse of the PDMS-based microfluidic microvalves discussed in this paper:

$$\Psi = \eta_1\frac{E_{bm}t_m{}^3g^2K_{post}K_{bilayer}}{\gamma L_e{}^4K_{AR}} \times \left[1+\eta_2\frac{\sigma_0}{E_{bm}}\left(\frac{L_e}{t_m}\right)^2+\eta_3\left(\frac{g}{t_m}\right)^2\right]. \qquad (3)$$

In eqn (3), γ is the interfacial adhesion energy, and η_1, η_2, and η_3 are constants that depend on the shape of the membrane and the boundary conditions. These constants can be analytically derived for simple shapes or determined experimentally.[20,21]

Applicability of the model to actuation in liquids: effect of fluid viscosity on membrane stiffness

In the expressions for membrane stiffness (eqn (1)), the effects of fluid viscosity were neglected. The force required for quasi-static compression of a fluid in an open channel is negligible, but the effect of fluid viscosity may be significant in the case of dynamic operation. In order to describe the influence of fluid viscosity on dynamic motion of the membrane, we assume the membrane motion to be damped by the fluid. This type of damping is known as squeeze film damping,[23] and accounts for the energy dissipation due to expansion and compression of viscous fluids between a fixed and vibrating flat plate. We include the effect of squeeze film damping in the expression for membrane stiffness (eqn (1)) by using an approximation of the Reynolds equation in fluid film lubrication[23,24] and neglecting the inertial effects of the fluid, as follows:

$$k = K_{bilayer}K_{post}\frac{K_{MS}}{K_{AR}}\left(K^1_{shape}\frac{E_{bm}t_m{}^3}{L_e{}^4}+K^2_{shape}\frac{\sigma_0 t_m}{L_e{}^2}\right)+k_{fluid}$$
$$k_{fluid} = \frac{96\mu L_e{}^2\omega}{\pi^4 g^3} \qquad (4)$$

where ω is the vibration frequency of the membrane, and μ is the dynamic viscosity of the fluid. Eqn (4) can be used to estimate the influence of fluid viscosity on dynamic operation of valves, by comparing the relative magnitudes of k_{fluid} and k. For instance, the effect of fluid viscosity would be significant during vibration of a typical PDMS-based microvalve in water at frequencies greater than 60 Hz. Here, we assume that the membrane is 500 μm in diameter and 10 μm thick, the channel height is 10 μm (typical dimensions of microvalves in microfluidic chips), and the material properties of PDMS are as listed in Table 3.

Applicability of the model to actuation in liquids: effect of flow pressure

The expressions for actuation potentials (eqn (2)) do not account for the flow pressure (p_{flow}). The electric field produced between the membrane and the fixed electrode will have to perform additional work against the flow pressure, which results in an increase in the actuation potentials. Using the principle of force balance, this increase in actuation potential (V_{flow}) is approximately given by:

$$V_{flow} = \sqrt{\frac{2p_{flow}\left(g+h_c\frac{\varepsilon_{fluid}}{\varepsilon_m}\right)^2}{\varepsilon_0\varepsilon_{fluid}}}. \qquad (5)$$

In the above expression, p_{flow} is the flow pressure relative to the atmosphere and is assumed to be constant along the surface of

the microvalve membrane. For any given situation of actuation of electrostatic microvalves, the additional potential required to actuate the microvalve due to the effects of flow pressure can be calculated using eqn (5) and compared to the actuation potentials calculated using eqn (2) to determine whether V_{flow} can be ignored or not.

Application of the analytical model to the design of electrostatic microvalves

In this section, we use the analytical model to design electrostatic microvalves with dimensions that can be feasibly fabricated with standard soft-lithographic techniques, can be actuated with low potentials, and do not collapse during fabrication and/or operation. We will specifically discuss the design of microvalves with circular membranes and will use the diameter, D, for the equivalent planar dimension, L_e, although the model can also be applied to design microvalves with rectangular membranes. The dimensions of the electrostatic microvalve that will be used in the discussion throughout this section are listed in Table 2, which correspond to typical dimensions in microfluidics. The post diameter was assumed to be 20% of the membrane diameter.

We assume the two layers of the bilayer membrane to be (1) a 1-μm thin insulating layer made out of PDMS ($t_2 = h_c = 1$ μm), and (2) a thicker backing layer of thickness t_m, also made out of PDMS. A few layers of multi-walled carbon nanotubes between the backing layer and the insulating layer form the top electrode. Thin layers of PDMS (<100 μm) are typically obtained by spinning PDMS on the desired substrate, which leads to thickness-dependent Young's modulus (lower thickness → higher modulus), due to reordering of the polymer chains during spinning to form stronger cross-linked networks.[25] Hence, a thickness-dependent Young's modulus will be assumed in this and later sections. The material properties of PDMS that will be used throughout this paper are listed in Table 3. The residual stresses in the membrane are assumed to be 0.04 MPa, which corresponds to the lowest residual stress measured in free-standing PDMS membranes.[26]

Critical design parameters

In this sub-section, we use the analytical model derived in the previous sections – eqn (1) and eqn (2) – to identify critical design parameters that influence the actuation potential. Table 4 lists the order of dependency of the actuation potential on different parameters (scaling relations), with higher order corresponding to greater influence. The data in Table 4 shows that the actuation potential is most sensitive to changes in membrane diameter D and membrane thickness t_m as expected. Less intuitive is the relation between the actuation potential and the dielectric properties of the fluid. Based on data in Table 4, an increase in the dielectric constant of the fluid will not necessarily decrease the actuation potential. This counter-intuitive observation is due to the fact that the dielectric constant of the conducting membrane in microfluidic microvalves (*e.g.*, $\varepsilon_m = 2.7$ for PDMS[28]) is not negligible compared to the dielectric constant of the fluid (*e.g.*, $\varepsilon_m = 80$ for water), whereas normally the dielectric constant of the top conducting layer is ignored ($\varepsilon_m = \infty$ for metals).[12]

Table 2 Typical dimensions of the electrostatic microvalves microfluidic devices

Parameter	Value (μm)
Diameter, D	100–1000
Membrane thickness, t_m	5–40
Channel height, g	2–20

Table 3 Material properties of PDMS

Property	Value
Young's modulus, E (MPa), thickness dependent	2–10[25]
Poisson's ratio, v	0.5[27]
Relative permittivity, ε	2.75[28]
Density, ρ / g cm^{-3}	0.95[29]

Dimensions of electrostatic microvalves that are feasible with respect to fabrication and operation

Using eqn (1), eqn (2) and eqn (3), we estimate the design parameter space for electrostatic microvalves with the following desirable specifications: (1) feasible from a fabrication point of view (range of microvalve dimensions in Table 2), (2) low actuation potentials (<300 V), and (3) no failure due to adhesion-driven collapse during fabrication and/or operation ($\Psi > 1$ in eqn (3)). Fig. 2 shows the design parameter space with respect to diameter, D, and channel height, g, for two different membrane thicknesses, t_m. The range of D and g, and the two extreme values for t_m (5 μm and 40 μm), are based on the dimensions listed in Table 2. The design parameter space (shaded region) is bounded by contour lines corresponding to actuation potential of 300 V, and lines corresponding to $\Psi = 1$. Note that the range for y-axes for the two plots in Fig. 2 are different, because the maximum allowable diameter (D) for any of the three fluids (air, oil, and water) is less than 600 μm for maximum gap value (g) of 20 μm for Fig. 2a, when t_m is 5 μm.

Along with air and water, we estimate the design parameter space for actuation in oil (3M™ Fluorinert FC-40), a commonly used liquid in microfluidic applications involving two-phase flows.[30] Also, the dielectric constant of oil ($\varepsilon_m = 2$[31]) is similar to that of air, while the interfacial adhesion properties in oil are expected to be similar to that in water. We assume that the interfacial adhesion energy, γ, for the PDMS-glass interface in air is 300 mJ m^{-2},[18] and is reduced by approximately an order of magnitude in liquids,[17,18] *i.e.*, $\gamma = 30$ mJ m^{-2} in oil and water. The shape constants for a fully clamped circular membrane of $\eta_1 = 40/3$, $\eta_2 = 51/160$, and $\eta_1 = 63/200$ were used in eqn (3).[21]

Table 4 Influence of various parameters on the actuation potential, scaling relations (higher order implies greater influence)

Parameter	Order of dependency
D	−2
t_m	2.5 for stable region, 3 for snap-in
g	0.5 for stable region, 1.5 for snap-in
ε	0.5 for stable region, 1 for snap-in

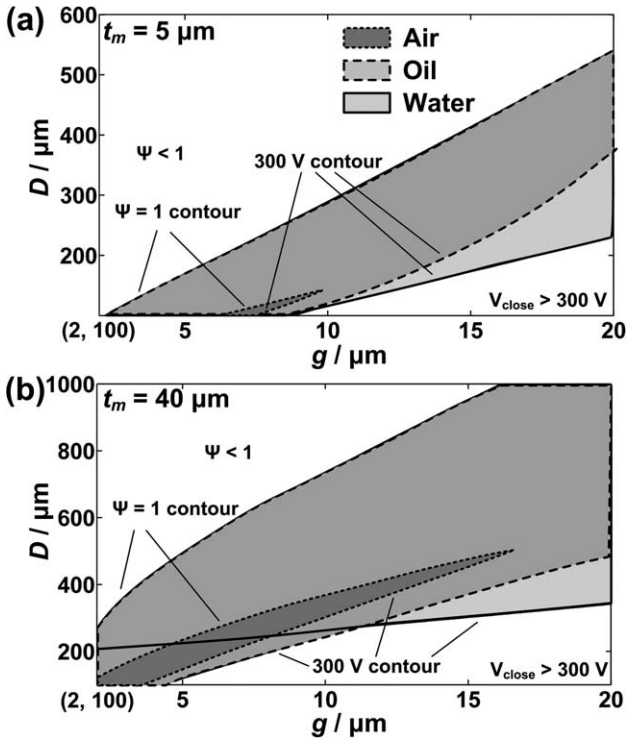

Fig. 2 Range of microvalve diameters and channel heights (shaded region) that can be actuated with potentials less than 300 V, while not collapsing during operation (*i.e.*, $\Psi > 1$), for two different membrane thicknesses: (a) $t_m = 5$ μm, (b) $t_m = 40$ μm. The design parameter space is estimated for air (darker), oil (hatched) and water (lighter).

In Fig. 2, the design parameter space for air is small compared to that for oil and water because of the higher interfacial adhesion energy in air, which increases the probability of the membrane to collapse. Note that the $\Psi = 1$ contour for oil and water are the same due to the same value of γ, while the 300 V contour lines for oil and air are close due to similar values for ε_m. Another interesting observation is that the design parameter space for air and water do not intersect in some regions (Fig. 2b), which implies that for certain microvalve geometries, reliable operation in both air and water is not possible. However, as mentioned before, even for microvalves that operate in aqueous solutions, adhesion-driven collapse in air is important for fabrication of these valves to avoid collapse of the valve membranes. Hence, techniques for minimizing adhesion without significantly influencing the membrane stiffness is crucial for fabrication and operation of electrostatic microvalves. One of these techniques is reduction of the interfacial adhesion energy (decreasing γ), *e.g.*, by the application of coatings with low surface energies, such as Teflon® and monolayers with pefluoro or hexadecyl end groups.[32]

Effect of residual stresses

Next, we used the analytical model to estimate the influence of residual stresses on the design parameter space of electrostatic microvalves. The fabrication of freestanding membranes results in residual stresses, which may significantly influence the stiffness of the membrane and consequently, the actuation potential and the elastocapillary number. To estimate the influence of residual stresses, we plot the design parameter space for the microvalves in Fig. 3, similar to that in Fig. 2, for two different values of residual stresses – zero and 0.04 MPa (lowest residual stress measured in free-standing PDMS membranes[26]). We plot the design parameter space for air and water only, for purposes of clarity.

The residual stresses in the membrane influence the design parameter space (Fig. 3). More importantly, minimizing the residual stresses reduces the values of the feasible diameters of the microvalves. For example, in Fig. 3a for a 20 μm channel height, the feasible microvalve diameters decrease from 200–550 μm for 0.04 MPa residual stress to 150–400 μm for zero stress. The reduced microvalve diameters will enable development of high-density microfluidic devices. This reduction in feasible diameter range is more evident for microvalves that can be actuated with lower potentials (figure in the supplementary information). Here, we assumed the residual stresses to be 0.04 MPa. In the supplementary information, we have included a comparison plot (Fig. S2) similar to Fig. 3, where we assumed the residual stresses to be 0.15 MPa, the maximum observed residual stresses in PDMS.

Residual stresses in PDMS membranes, freestanding and on a substrate, have been measured to be in the range of 0.04–0.15 MPa.[26,33] This implies that residual stresses will influence the design parameter space of electrostatic microfluidic microvalves fabricated out of PDMS, as studied here. Ideally, these residual stresses need to be minimized to decrease the actuation potential and to enable high-density integration of microvalves. Residual stresses in freestanding films are often caused by a mismatch of

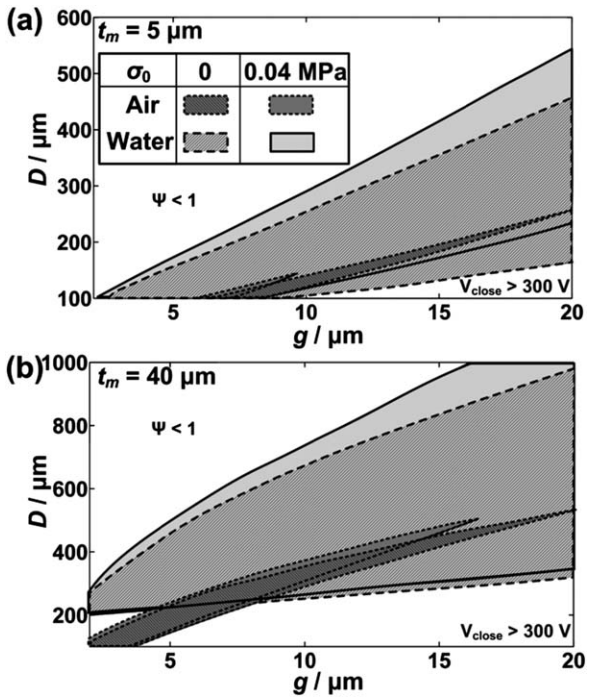

Fig. 3 Design parameter space for microvalves for two different values of residual stresses. The design space is estimated for two different membrane thicknesses: (a) $t_m = 5$ μm, (b) $t_m = 40$ μm, and two different values of residual stresses (0 and 0.04 MPa).

thermal expansion coefficients between the film and the substrate. Hence, curing the PDMS structures at room temperature, rather than elevated temperatures, may reduce the residual stresses. However, room temperature curing of PDMS will lead to prolonged curing, and hence time-dependent material properties. To avoid the issues with prolonged curing, the PDMS structures should be cured and the various layers assembled at room temperature to minimize residual stress. Then, the assembled device should be tempered at 200 °C for 4 h, which has been shown to ensure that the PDMS is completely cured, and that the mechanical properties of PDMS remain constant over time.[34]

Fabrication and testing of the electrostatic microvalves

In order to experimentally verify the analytical model described in previous sections, we tested an array of electrostatic microvalves actuated in air and oil. We preferred oil as an example of a liquid system over water, since the conducting properties of water necessitates high frequency potentials (>10 MHz) for actuation,[35] which requires specialized equipment for high-frequency voltage generation. In addition, a class of applications involving two-phase flows, *e.g.*, droplet-based microfluidics, require oil as the carrier liquid.[30] In recent years, droplet-based microfluidics has received increased attention in the fields of biological and chemical synthesis and analysis, due to the advantages of efficient mixing, reduced dispersion of reagents, and the ability to perform parallel experiments.[2,36] Electrostatic microvalves that can route water droplets in oil will not only enhance the capabilities of droplet-based microfluidics, but also provide additional advantages of increased density and portability.

We used soft-lithographic techniques, a combination of photolithography and replica molding, to fabricate the main structural elements of the microvalve, which includes an insulating layer, a conducting layer and a microfluidic channel. The insulating layer and the microfluidic channel were fabricated by firstly spinning PDMS on the master of the microfluidic channel, curing the PDMS, and removing the PDMS mold from the master. A few layers of multi-walled carbon nanotubes (CNT) were deposited on top of the insulating layer to form the top electrode. Finally, a thick layer of PDMS was spun and cured on the insulating layer to serve as the backing layer, which enhances the robustness and facilitates convenient handling of the conducting membrane. Details of the fabrication procedures for the electrostatic microvalves are discussed in the supplementary information. A thin film of conducting material, indium tin oxide (ITO), was deposited on a glass slide to create the bottom electrode. For the electrical contacts, a mixture of CNT and PDMS (~10% CNT by weight) was used to contact the top electrode (CNT layer), while an alligator clip was used to contact the bottom electrode (ITO on glass). To actuate the microvalves, we applied a potential between the two electrodes using a DC power source. Optical micrographs of open and closed electrostatic microvalves are shown in Fig. S4 in the supplementary information.

We tested arrays of circular microvalves with three different channel heights, g, (2, 4 and 7 μm), two different thicknesses, t_m, (25 and 35 μm), and eight different diameters, D, (200–900 μm) to study the influence of microvalve geometry on actuation potentials in air and oil (3M™ Fluorinert FC-40 oil). The thickness of the insulating layer, h_c, varied between 2 to 5 μm depending on the dimensions of the microvalve, while the diameter of the post was 20% of the membrane diameter. The overall thickness of the PDMS membrane and the thickness of the insulating layer were measured using scanning electron microscopy, while the membrane diameter and channel height were measured using an optical microscope and a profilometer, respectively.

Fig. 4 shows the comparison between analytical predictions (eqn (1) and (2)) and experimental data for actuation potentials. Microvalves with geometries above the dashed lines are analytically predicted to not collapse during fabrication and operation (eqn (3)), *i.e.*, $\Psi > 1$; a circle around the data point indicates a valve that was experimentally observed to reopen after the actuation potential was removed. Each data point and the error bar indicate the average value obtained from three separate microvalves and the standard deviation, respectively.

The lowest observed actuation potential for a valve that reopened was 110 V for a microvalve with a diameter of 200 μm, thickness 25 μm, and a channel height of 4 μm. Also, most of the valves snapped close into contact with the channel floor after a certain threshold potential, which we assumed to be the actuation potential. This snap-in behavior is due to the fact that the microvalve actuation is governed by pull-in instability, as predicted by the analytical model (eqn (2)). We observed good agreement between experimentally observed potential values and analytically predicted values, with the deviation being between 7% and 30% in most cases. The deviation was higher for microvalves actuated in oil with 2 μm channel height (40 to 50%), which probably is due to the premature collapse of the valves for low channel heights in liquds caused by surface tension. Some of the observed deviation can be attributed to the fact that the variation in dimensions (g, t_m, h_c) among different valves (fabrication inconsistency) affect the measured actuation potentials. Similarly, the assumptions in deriving the expressions for actuation potentials and more importantly, the values of material properties from literature (*e.g.*, Young's modulus and adhesion energies) influence the analytically predicted values. Also, the higher observed actuation potentials for some of valves could be due to the relatively large resistance of the nanotube film (~4 kΩ) that will result in a potential drop across the electrodes, which is not accounted for in the analytical model.

The occurrence of leakage, typically resulting from incomplete closure of the valve, can be an important issue when using microvalves in microfluidic applications. We observed that 85% of the valve seat was occupied by the valve membrane, indicating almost complete closure, and hence minimum leakage. A more detailed experimental characterization of leakage in electrostatic microvalves has been carried out by Yildrim and Kulah.[37] These microvalves were fabricated out of parylene, a stiffer polymer than PDMS. We expect valve closure to be better, and hence leakage to be less of an issue for the valves reported here.

In summary, these preliminary experimental results validate the applicability of the analytical model to quantitatively predict actuation potentials for different microvalve geometries. The experimental data is primarily discussed to highlight the application of the model to quantitatively predict actuation potentials in air and liquids, and a more extensive experimental study with

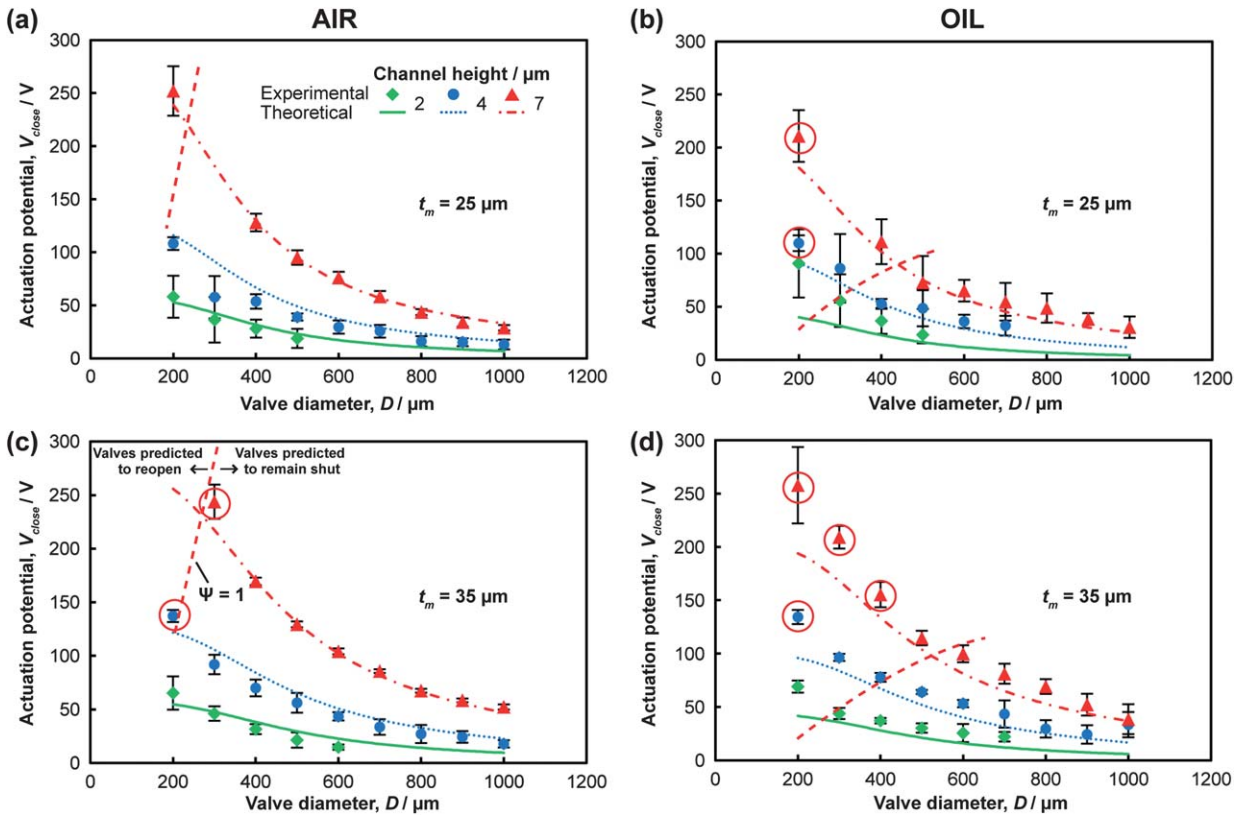

Fig. 4 Comparison between actuation potentials (solid, dotted, and dash-dotted lines) predicted with the analytical model and those determined experimentally for microvalves of different diameters with three different channel heights, 2, 4 and 7 μm, and two different thicknesses actuated in air and oil. (a) $t_m = 25$ μm in air, (b) $t_m = 25$ μm in oil, (c) $t_m = 35$ μm in air, and (d) $t_m = 35$ μm in oil. The valves above the dashed lines (going from bottom-left to top-right) are analytically predicted to reopen after the actuation potential was removed, while the circle around the data point indicates the valve that was observed to experimentally reopen. Three valves were tested per data point, and each valve was tested thrice.

fabrication and valve characterization details will be presented in a future publication.

Design guidelines and operational considerations for electrostatic microvalves

Based on the analytical model described in the previous sections, we developed a set of design guidelines and operational considerations for electrostatic microvalves in microfluidic applications as follows:

1. After identifying the range of permissible microvalve dimensions, which is determined by the feasibility of fabrication procedures and the requirements of the end-application, the model can be used to generate contour plots corresponding to the desired actuation potential and $\Psi = 1$. The area bounded by the two contour lines (Fig. 2) represent the design parameter space that correspond to dimensions of microvalves, which can be actuated with low potentials and not collapse due to interfacial adhesion. Since the devices with microvalves will be assembled under ambient conditions, a more accurate design parameter space is obtained by considering the $\Psi = 1$ contour line for air, as the membranes are more prone to collapse in air than liquids.

2. Residual stresses in the microvalve membrane not only increase the membrane stiffness of thin polymeric membranes, but also increase the values of feasible valve dimensions. Strategies for reducing residual stresses, such as room temperature curing of the polymer followed by tempering of the assembled device at high temperatures, are critical towards reliable and robust operation of the microvalves at low actuation potentials in dense microfluidic networks.

3. Microvalve operation in the regime governed by pull-in instability is desirable because in that case, the actuation potential needs to be only large enough to deflect the valve membrane to the point of the critical deflection. As a result, the power requirement for the microvalve operation is reduced as opposed to the case where the microvalve operation is in the stable deflection regime. The geometrical parameters of the microvalve and, to some extent, the relative permittivity of the membrane material can be adjusted to ensure that the microvalve operation is governed by pull-in instability.

4. The conducting layer should be as thin as possible to minimize the increase in membrane stiffness due to the stiffness of the conducting layer. However, the conducting layer should also be continuous, since a discontinuous film has a higher resistance which will result in increased actuation potentials.[38] A method to minimize the effect of discontinuous films on electrical conductivity is to introduce compressive stresses in the films, which will tend to close up the cracks.

5. The high electrical fields in electrostatic microfluidic valves (~1 MV m^{-1}) could result in parasitic charging at the

membrane-fluid interface.[39–41] These parasitic charges could result in up to 100% increase in the actuation potentials compared to analytically predicted values.[41] Hence, strategies to reduce the effect of parasitic charging at the membrane-fluid interface, such as reversal of polarity of the electrodes after every actuation,[41] will result in lower actuation potentials.

Application of the electrostatic valves in microfluidic devices

Following the design rules described above, the electrostatic valves designed for low actuation potentials (<300 V) can be used in microfluidic devices that operate at low pressures or flow rates. In case of high pressure flows, eqn (5) predicts the increase in actuation potentials for different flow rates and channel dimensions. For instance, for a microvalve with $g = 10$ μm and $h_c = 1$ μm actuated in water, the approximate increase in potential per unit flow pressure is 170 V/Pa. This increase in potential can be reduced by using lower channel heights (decreasing g in eqn (5)), but the smaller channel heights significantly increase the hydraulic resistance of the channel and consequently limit the maximum permissible flow rate. For example, in prior work, the maximum flow rate successfully achieved in microfluidic devices employing electrostatic valves was less than 2 nL min^{-1}.[6,7] The lower limits on flow pressure and flow rates that can be used in combination with electrostatic valves is a known, inherent problem.[39] This issue is even more pronounced when low actuation potentials are desired. One approach to address this issue involves the use of a pneumatic pressure-balanced electrostatic valves to operate at higher flow pressures.[39,42] In these type of valves, the flow pressure is balanced either internally by the flow itself, or externally by a separate pneumatic line. The electrostatic actuation is used to only open or close the valve, but not to perform work against the flow pressure.

The electrostatic microvalves discussed here can also be applied in the following three scenarios in microfluidics. (1) Complementary to continuous flow microfluidics, 'digital microfluidics' involving manipulation of quantized volumes (*e.g.*, droplets) is an emerging area of research.[43] In some of these applications (*e.g.*, the study of long duration on-chip chemical reactions[44]), the liquids are manipulated in a quasi-static manner (discretized), and hence, the flow rates are very low. The electrostatic microvalves described in this paper will greatly enhance the automation capabilities and portability of these digital microfluidic applications. (2) In microfluidic devices using pneumatic valves, the pneumatic lines required for operating the valves are controlled by externally connected solenoid valves, which limit the scalability of the microfluidic device due to constraints on the number of peripheral connections.[45] These solenoid valves can be replaced by on-chip electrostatic microvalves controlled by ICs, which will reduce the size of the ancillaries and enhance scalability. (3) Normally closed valves are advantageous compared to the standard normally open valves (Fig. 1) in applications requiring continuous closed state of valve operation.[46] If these valves could be operated by electrostatic actuation as opposed to pneumatic actuation, the microfluidic devices using these valves will require compact ancillaries. The analytical model derived here is valid for designing electrostatic microvalves in the all of the above scenarios. Note that in the last two scenarios, electrostatic actuation does not occur in water, which avoids the water-associated issues of electric double layer formation. The use of electrostatic valves in combination with aqueous solutions will be discussed in the next sub-section.

Application of the electrostatic valves in aqueous solutions

For aqueous solutions, the applied electric field needed to actuate the valves results in the formation of an electric double layer (EDL) that effectively shields the applied potential.[11,35] To avoid the formation of an EDL, an alternating or AC potential, rather than a constant DC potential, can be applied to still actuate the microvalve. The frequency of the AC potential (f_{AC}) required to actuate the microvalve depends on the geometry of the microvalve and the conductivity of the liquid.[35] This frequency is directly proportional to h_c/g,[35] *e.g.*, for the PDMS-based microvalve discussed here with $g = 10$ μm and $h_c = 1$ μm, f_{AC} is approximately 2 MHz.

The expressions to predict actuation potentials reported above (eqn (2)) are still valid when using AC potentials. In this case, the induced electrostatic force is the sum of a static force and a force at a frequency of $2f_{AC}$. If the mechanical response of the microvalve at frequency $2f_{AC}$ is negligible compared to the response at the microvalve resonance frequency ($f_{resonance}$), *i.e.*, $2f_{AC} > f_{resonance}$, then the potential needed to actuate a valve (V_{close}) will be equal to the root mean square (rms) value of the applied AC potential (V_{rms}).[11] For a typical PDMS microvalve, the resonant frequency is approximately 5 kHz (see supplementary information), which is lower than $2f_{AC}$ for most liquids.[11,35] Thus, the above condition for replacing V_{close} by V_{rms} is satisfied, as implemented in previous sections for predicting actuation potentials in water based on the model reported here.

Generation of AC potentials with high frequencies (>1 MHz), especially at voltage values needed for electrostatic actuation of microvalves (>50 V), requires specialized bulky equipment. The required frequency f_{AC} can be reduced by decreasing h_c or increasing g. However, fabrication limitations imposed by soft lithography ($h_c > 1$μm) and limits on the maximum actuation potential as determined by the microvalve dimensions ($g < 20$ μm) place constraints on the minimum allowable value for f_{AC}. In summary, use of the electrostatic microvalves reported here in portable microfluidic applications involving aqueous solutions is limited due to the need for of specialized bulky ancillaries.

Conclusion

In this paper, we used a parallel-plate capacitor model in conjunction with plate theory to develop an analytical model to describe the operation of electrostatic microvalves in microfluidic applications. Based on this analytical model, we identified critical design parameters and estimated design parameter space with respect to microvalve dimensions and material properties to ensure reliable microvalve operation at low actutation potentials. We discussed the electrostatic actuation in terms of several microscale phenomena, such as snap-in dynamics due to the unstable equilibrium between mechanical and electrostatic forces, squeeze film damping as a result of high fluid viscosity, and collapse of valves due to adhesion. To validate the analytical

model, we fabricated arrays of microvalves of different dimensions and tested these for actuation in air and oil. The experimental observations were in qualitative and quantitative agreement with the analytical model. Based on the analytical model, we derived a set of design guidelines and operational considerations that can be used to minimize the actuation potential of electrostatic microvalves in microfluidic applications while maintaining feasibility of fabrication and operation.

In this paper, the analytical model was discussed specifically with respect to the design of electrostatic microvalves in PDMS-based microfluidic structures. However, the model can also be used in the design of microfluidic components, such as peristaltic pumps, in which dynamic actuation of a series of valves is important, and the equations describing membrane mechanics can also be used in the design of the presently more commonly used pneumatic microvalves. Further research, guided by the analytical model presented in this paper, is needed in the design and fabrication of electrostatic microvalves that can be integrated in very large scale integrated microfluidic networks with similar ease and density as the more prevalent pneumatic microvalves.

Acknowledgements

We gratefully acknowledge financial support from the Department of Energy (DOE) through the National Institute for NanoEngineering (NINE) initiative of the Lab Directed Research and Development (LDRD) program at Sandia National Laboratories. This work was partially supported by the National Center for Supercomputing Applications (NCSA) under proposal number MSS080036 and utilized the SGI-Altix (Cobalt) for FEA simulations. Scanning electron microscopy and profilometry was carried out in part in the Frederick Seitz Materials Research Laboratory Central Facilities, University of Illinois, which are partially supported by the U.S. Department of Energy under grants DE-FG02-07ER46453 and DE-FG02-07ER46471. We also thank Dr R.C. Givler and Dr G.A. Ten Eyck from Sandia National Laboratories for stimulating discussions, and Tom Bassett from the University of Illinois for his help in fabrication and characterization of some of the valves.

References

1 R. G. Blazej, P. Kumaresan and R. A. Mathies, *Proc. Natl. Acad. Sci. U. S. A.*, 2006, **103**, 7240–7245; C.-C. Lee, G. Sui, A. Elizarov, C. J. Shu, Y.-S. Shin, A. N. Dooley, J. Huang, A. Daridon, P. Wyatt, D. Stout, H. C. Kolb, O. N. Witte, N. Satyamurthy, J. R. Heath, M. E. Phelps, S. R. Quake and H.-R. Tseng, *Science*, 2005, **310**, 1793–1796; R. Pal, M. Yang, R. Lin, B. N. Johnson, N. Srivastava, S. Z. Razzacki, K. J. Chomistek, D. C. Heldsinger, R. M. Haque, V. M. Ugaz, P. K. Thwar, Z. Chen, K. Alfano, M. B. Yim, M. Krishnan, A. O. Fuller, R. G. Larson, D. T. Burke and M. A. Burns, *Lab Chip*, 2005, **5**, 1024–1032.
2 C. B. Rohde, F. Zeng, R. Gonzalez-Rubio, M. Angel and M. F. Yanik, *Proc. Natl. Acad. Sci. U. S. A.*, 2007, **104**, 13891–13895.
3 M. A. Unger, H. P. Chou, T. Thorsen, A. Scherer and S. R. Quake, *Science*, 2000, **288**, 113–116.
4 K. W. Oh and C. H. Ahn, *J. Micromech. Microeng.*, 2006, **16**, R13–R39.
5 S. Prakash, M. B. Karacor and S. Banerjee, *Surf. Sci. Rep.*, 2009, **64**, 233–254.
6 M. P. Chang and M. M. Maharbiz, *Lab Chip*, 2009, **9**, 1274–1281.
7 J. Xie, J. Shih, Q. Lin, B. Yang and Y.-C. Tai, *Lab Chip*, 2004, **4**, 495–501.
8 G. Flores, G. Mercado, J. A. Pelesko and N. Smyth, *SIAM J. Appl. Math.*, 2007, **67**, 434–446; Y. Guo, Z. Pan and M. J. Ward, *SIAM J. Appl. Math.*, 2005, **66**, 361.
9 N. C. Goulbourne, M. I. Frecker and E. Mockensturm, *Smart Structures and Materials 2004: Electroactive Polymer Actuators and Devices (EAPAD)*, San Diego, CA, USA, 2004.
10 C. Wang, W. Guo and Q. Feng, *Acta Mechanica*, 2005, **180**, 49–60.
11 A. S. Rollier, B. Legrand, D. Collard and L. Buchaillot, *J. Micromech. Microeng.*, 2006, **16**, 794–801.
12 P. M. Osterberg and S. D. Senturia, *J. Microelectromech. Syst.*, 1997, **6**, 107–118.
13 S. Timoshenko and S. Woinowsky-Krieger, *Theory of Plates and Shells*, McGraw-Hill Book Company, New York, 1959.
14 M. D. Giovanni, *Flat and Corrugated Diaphgram Design Handbook*, Marcel Dekker Inc., New York, 1982.
15 M. K. Small and W. D. Nix, *J. Mater. Res.*, 1992, **7**, 3242–3249; J. J. Vlassak and W. D. Nix, *J. Mater. Res.*, 1992, **7**, 3242–3249.
16 W. C. Young, *Roark's formulas for stress and strain* McGraw-Hill, New York, 2002.
17 K. J. Hsia, Y. Huang, E. Menard, J. U. Park, W. Zhou, J. Rogers and J. M. Fulton, *Appl. Phys. Lett.*, 2005, **86**, 154106–154103.
18 K. G. Sharp, G. S. Blackman, N. J. Glassmaker, A. Jagota and C.-Y. Hui, *Langmuir*, 2004, **20**, 6430–6438.
19 M. P. de Boer and T. A. Michalske, *J. Appl. Phys.*, 1999, **86**, 817–827; R. Maboudian and R. T. Howe, *J. Vac. Sci. Technol., B*, 1997, **15**, 1–20; E. E. Parker, W. R. Ashurst, C. Carraro and R. Maboudian, *J. Microelectromech. Syst.*, 2005, **14**, 947–953.
20 C. H. Mastrangelo and C. H. Hsu, *J. Microelectromech. Syst.*, 1993, **2**, 33–43.
21 C. H. Mastrangelo and C. H. Hsu, *J. Microelectromech. Syst.*, 1993, **2**, 44–55.
22 Z. Yapu, *Acta Mech. Sin.*, 2003, **19**, 1–10.
23 S. D. Senturia, Kluwer Academic Publishers, New York, 2001, pp. 334–339.
24 R. B. Darling, C. Hivick and J. Xu, *Sens. Actuators, A*, 1998, **70**, 32–41; B. J. Hamrock, Mc-Graw Hill, New York, 1994, pp. 117–166, 277–292.
25 M. Liu, J. Sun, Y. Sun, C. Bock and Q. Chen, *J. Micromech. Microeng.*, 2009, **19**, 035028.
26 A. Thangawng, R. Ruoff, M. Swartz and M. Glucksberg, *Biomed. Microdevices*, 2007, **9**, 587–595.
27 D. Armani, D. Armani, C. Liu and N. Aluru, *Twelfth IEEE International Conference on Micro Electro Mechanical Systems*, MEMS '99., 1999.
28 D. Corning, Dow Corning, 2008.
29 J. E. Mark, *Polymer Data Handbook*, Oxford University Press, New York, 1999.
30 D. Chatterjee, B. Hetayothin, A. R. Wheeler, D. J. King and R. L. Garrell, *Lab Chip*, 2006, **6**, 199–206.
31 3M, Dow Corning, 2010.
32 L. Yang, N. Shirahata, G. Saini, F. Zhang, L. Pei, M. C. Asplund, D. G. Kurth, K. Ariga, K. Sautter, T. Nakanishi, V. Smentkowski and M. R. Linford, *Langmuir*, 2009, **25**, 5674–5683.
33 M. Maghribi, J. Hamilton, D. Polla, K. Rose, T. Wilson and P. Krulevitch, *2nd Annual International IEEE-EMB Special Topic Conference on Microtechnologies in Medicine & Biology* 2002.
34 F. Schneider, T. Fellner, J. Wilde and U. Wallrabe, *J. Micromech. Microeng.*, 2008, **18**, 065008.
35 T. L. Sounart, T. A. Michalske and K. R. Zavadil, *J. Microelectromech. Syst.*, 2005, **14**, 125–133.
36 A. Huebner, S. Sharma, M. Srisa-Art, F. Hollfelder, J. B. Edel and A. J. deMello, *Lab Chip*, 2008, **8**, 1244–1254; Y.-S. Yu and Y.-P. Zhao, *J. Colloid Interface Sci.*, 2009, **332**, 467–476; J. L. Gardea-Torresdey, K. J. Tiemann, G. Gamez, K. Dokken, S. Tehuacanero and M. José-Yacamán, *J. Nanopart. Res.*, 1999, **1**, 397–404.
37 E. Yıldırım and H. Kulah, *J. Micromech. Microeng.*, 2011, **21**, 105009.
38 M. R. Begley, H. Bart-Smith, O. N. Scott, M. H. Jones and M. L. Reed, *J. Mech. Phys. Solids*, 2005, **53**, 2557–2578.
39 W. van der Wijngaart, H. Ask, P. Enoksson and G. Stemme, *Sens. Actuators, A*, 2002, **100**, 264–271.
40 J. Wibbeler, G. Pfeifer and M. Hietschold, *Sens. Actuators, A*, 1998, **71**, 74–80.
41 T.-J. Yao, K. Walsh and Y.-C. Tai, *The Fifteenth IEEE International Conference on Micro Electro Mechanical Systems*, 2002.

42 B. Bae, J. Han, R. I. Masel and M. A. Shannon, *J. Microelectromech. Syst.*, 2007, **16**, 1461–1471; K. Yoshida, Y. Hagihara, S. Tanaka and M. Esashi, *Micro Electro Mechanical Systems, 2006*. MEMS 2006 Istanbul. 19th IEEE International Conference on, 2006.
43 J. P. Urbanski, W. Thies, C. Rhodes, S. Amarasinghe and T. Thorsen, *Lab Chip*, 2006, **6**, 96–104.
44 M. R. Thorson, S. Goyal, B. R. Schudel, C. F. Zukoski, G. G. Z. Zhang, Y. Gong and P. J. A. Kenis, *Lab Chip*, 2011, **11**, 3829–3837.
45 M. C. Cole, A. V. Desai and P. J. A. Kenis, *Sens. Actuators, B*, 2011, **151**, 384–393.
46 R. Mohan, B. R. Schudel, A. V. Desai, J. D. Yearsley, C. A. Apblett and P. J. A. Kenis, *Sensors and Actuators B: Chemical*, 2011, **160**, 1216–1223; B. R. Schudel, C. J. Choi, B. T. Cunningham and P. J. A. Kenis, *Lab Chip*, 2009, **9**, 1676–1680; B. R. Schudel, M. Tanyeri, A. Mukherjee, C. M. Schroeder and P. J. A. Kenis, *Lab Chip*, 2011, **11**, 1916–1923.